View metadata, citation and similar papers at core.ac.uk
brought to you by CORE
provided by idUS. Depósito de Investigación Universidad de Sevilla

Liquid methanol Monte Carlo simulations with a refined potential which includes polarizability, nonadditivity, and intramolecular relaxation

Maximiliano Valdéz-González,[a] Humberto Saint-Martin, and Jorge Hernández-Cobos
Instituto de Ciencias Físicas, Universidad Nacional Autónoma de México, Apartado Postal 48-3, 62251 Cuernavaca, Morelos, Mexico

Regla Ayala and Enrique Sanchez-Marcos
Departamento de Química Física, Universidad de Sevilla, 41012-Sevilla, Spain

Ivan Ortega-Blake[b]
Departamento de Física Aplicada, Cinvestav, Km. 6 Antigua Carretera a Progreso, Cordemex, Mérida 97310, Yucatán, Mexico

Received 9 March 2007; accepted 2 October 2007; published online 12 December 2007

Monte Carlo simulations of liquid methanol were performed using a refined ab initio derived potential which includes polarizability, nonadditivity, and intramolecular relaxation. The results present good agreement between the energetic and structural properties predicted by the model and those predicted by ab initio calculations of methanol clusters and experimental values of gas and condensed phases. The molecular level picture of methanol shows the existence of both rings and linear polymers in the methanol liquid phase. © 2007 American Institute of Physics.
DOI: 10.1063/1.2801538

I. INTRODUCTION

Nowadays it is possible to use refined potentials in numerical simulations of physicochemical systems involving small molecules[1–3] and attain sufficiently good agreement with the experimental observations. The reliability that such validation confers upon the simulations allows for the construction of a molecular image that contributes to a better understanding of the phenomena. It seems that construction of refined potentials requires paying attention to molecular properties such as polarizability, intramolecular relaxation, and nonadditivity.[4–7] These flexible potentials can be adjusted to ab initio data of the molecule and the intermolecular interaction, with no reference to a particular thermodynamic state of the condensed phase, allowing for its unbiased use in any condition. A great effort has been made for the development of water potentials[1,4,8–10] and in some cases for other small molecules.[11,12] It is indeed convenient to extend the use of this tool to other systems and also to determine to what extent the inclusion of different molecular properties that add dearly to the computational cost is required for the proper reproduction of the experimental data.[13]

Liquid methanol is of great interest given its many uses, particularly that as a common organic solvent and more recently as an important fuel alternative.[14] Additionally, a lot of work has been devoted to the understanding of its unusual physical properties[15] that have been associated with a peculiar molecular behavior that is conducive to methanol being certainly one of the most structured liquids. In the crystal phase methanol presents long one-dimensional chains of hydrogen bonds.[16,17] It has therefore been thought that something similar could be occurring in the liquid phase and be responsible for its peculiar behavior. Several numerical simulations[18–23] and neutron diffraction experiments[24–26] have produced data that support this view. On the other hand, experimental results of neutron diffraction,[27,28] x-ray scattering,[29,30] and x-ray emission spectroscopy[31] have been taken to support the existence of cyclic clusters of methanol in the liquid phase. Kashtanov et al.[31] have suggested that numerical simulations could be using potentials that are not able to reproduce the hydrogen bonding network in ring structures. There is a substantial number of numerical simulations of methanol[18–23,32–34] and some of them which include polarizability[35–38] have shown the need for refined potentials.

In this work a refined methanol-methanol potential that uses the mobile charge densities in harmonic oscillators (MCDHO) model[4] which includes polarizability, nonadditivity, and intramolecular relaxation is presented. The potential is adjusted to ab initio surfaces and tested in the reproduction of ab initio methanol clusters, their energies, and structures. The potential is then used in Monte Carlo simulations of liquid methanol. This serves to test the potential and determine the validity of its use. In addition we tested how accounting for different molecular properties, such as polarizability and intramolecular relaxation, affects the reproduction of the experimental properties. The quality of the potential helps us to further the understanding of the behavior of liquid methanol.

[a]Electronic mail: maxvalde@fis.unam.mx
[b]On leave from Instituto de Ciencias Físicas, Universidad Nacional Autónoma de México.

 © 2007 American Institute of Physics
Reuse of AIP Publishing content is subject to the terms: https://publishing.aip.org/authors/rights-and-permissions. Downloaded to IP: 150.214.182.116 On: Wed, 19 Oct 2016 14:19:58

TABLE I. Structural parameters for the minimum energy methanol monomer predicted at the MP2 and QCC levels. Distances are in angstroms, bond and dihedral angles are in degrees, and dipole moment in Debye.

Method	r(CO)	r(OH)	∠(COH)	d(HCOH)	μ
MP2/cc-pvDZ	1.4171	0.9656	106.3	179.88	1.63
MP2/6-31++G**	1.4290	0.9644	108.5	179.88	1.99
MP2/6-311++G**	1.4217	0.9544	107.3	179.88	1.93
MP2/aug-cc-pVDZ	1.4342	0.9659	107.9	180.00	1.71
MP2/cc-pvTZ	1.4188	0.9594	107.4	179.83	1.65
MP2/aug-cc-pvTZ	1.4239	0.9611	108.0	179.81	1.70
MP2/cc-pVQZ	1.4177	0.9577	108.0	179.83	1.68
MP2/aug-cc-pVQZ	1.4353	0.9658	107.9	179.6	1.70
QCC TZV(2p,2d)+[a]	1.4286	0.9583	107.6	180.0	1.81

[a]Reference 34.

II. METHODS

A. Potential energy surfaces

The methanol-methanol potential was developed by reproducing ab initio energy surfaces for the intramolecular relaxation, the dipole moments of different methanol structures, the pairwise interaction, and the nonadditive terms of the intermolecular interaction. Molecular orbital calculations for all cases were done with the GAUSSIAN98 program.[39] We considered in the calibration procedure Gaussian basis sets 6-31++G** and 6-311++G** and correlation-consistent basis sets cc-pVDZ, aug-cc-pVDZ, cc-pVTZ, and cc-pVQZ.[40–42]

Of course a compromise has to be made between the computational cost and the quality of the molecular calculation due to the fact that a great number of structures need to be considered. Hence, in order to determine the optimal level of calculation we looked into the prediction of various properties reported at different levels of molecular theory. Table I shows the optimal structures for the monomer of methanol predicted with different basis set sizes at the MP2 and QCC levels. It is clear that there is a fast convergence of the structural parameters and that the aug-cc-pVDZ basis set yields a good approximation to more expensive and complete basis sets. In a previous study Wang et al. compared the vibrational spectra of methanol predicted with different basis sets.[43] It was found that a basis set of similar size yielded a reasonable approximation to the experimental spectra. The dipole moment shows more discrepancy, with a value 10% larger for the most extended basis set. However, since the value predicted by the aug-cc-pVDZ basis set is closer to the experimental dipole moment[44] of 1.69 D, we decided to use this basis set for the description of the intramolecular surface.

Table II shows the structural parameters of the optimal methanol dimer predicted by different basis sets. It is clear that there is convergence in the predicted dimer configuration. The corresponding energies are also presented and compared to other data in the literature. The values corresponding to the three largest basis sets were computed with structures optimized with a 6-31++G** basis set and monomers kept frozen in the dimer optimization.[45] Even if they are not fully comparable they provide a good reference point on the expected convergence value, and since they correspond to a partial optimization it is clearly a lower limit. The optimal dimers for the six smaller basis sets were optimized in their own basis set and counterpoise (CP) correction ap-

TABLE II. Structural parameters of the optimal methanol dimer predicted at the MP2 level (left columns). Distances are in angstroms, and bond and dihedral angles are in degrees. Predicted interaction energy (kcal/mol) for the optimal methanol dimer at the MP2 and CCSD(T) limit levels (right columns). E_{int} corresponds to the energy of the dimer minus the energy of the relaxed monomers, E_{def} is the deformation energy, and $E_{int}=E_{int}+E_{def}$ is the interaction energy. The relative time for a single point calculation for each basis set is also presented.

Basis set	r O··H	r O··O	∠ OH··O	∠ HO··H	d COH··O	d OH··OC	E_{int}	E_{def}	E_{int}	Rel. time
cc-pVDZ	1.887	2.819	159.3	101.7	109.1	−20.7	−3.53	0.20	−3.33	1.0
6-31++G**	1.887	2.853	172.5	117.9	109.0	16.9	−5.22	0.11	−5.11	1.5
6-311++G**	1.886	2.846	171.9	122.5	98.3	30.0	−4.97	0.11	−4.86	5.9
aug-cc-pVDZ	1.887	2.847	168.2	112.7	132.3	−6.7	−5.22	0.11	−5.11	15.7
cc-pVTZ	1.872	2.802	160.4	131.0	97.8	24.9	−5.09	0.19	−4.90	39.0
aug-cc-pVTZ	1.877	2.836	169.4	117.0	129.9	1.0	−5.60	0.11	−5.49	3486.3
cc-pVQZ									−5.21[a]	—
cc-pV5Z									−5.39[a]	—
CCSD(T) limit									−5.45[a]	—

[a]Reference 45.
[b]aug-cc-pVTZ optimized geometry.

Reuse of AIP Publishing content is subject to the terms: https://publishing.aip.org/authors/rights-and-permissions. Downloaded to IP: 150.214.182.116 On: Wed, 19 Oct 2016 14:19:58

plied to the energy obtained by subtracting the relaxed methanol energies. The convergence limit has also been validated by comparison to the experimentally derived binding energy.[46] With this in mind, we can estimate that the value obtained by the aug-cc-pVDZ basis set has a small underestimation of 5% and considering the relative computational costs presented in Table II, the aug-cc-pVDZ basis set was chosen for the determination of the dimer interaction energy at the MP2 CP corrected level.

Since CP correction applied to fully optimized dimers including monomer relaxation is not well defined, we performed the following algorithm for the estimation of CP correction at the aug-cc-pVDZ basis set level. The dimer interaction was computed by subtracting the energies of the resulting methanol monomers in the fully optimized dimer from the energy of the dimer. The energies of these monomers were computed in the complete basis of the dimer. Then the deformation energy of each of these monomers with respect to the optimal one was computed in the same basis set and subtracted from the previous energy; using a much larger basis set as the aug-cc-pVQZ did not produce any significant difference in the deformation energy values. This algorithm allows for a better search of the optimal structure that does not necessarily correspond to the minimum of the energy surface computed ab initio, due to CP correction. Of course it is possible that CP overcorrects the interaction energy, but since CP is in itself small, this effect is negligible.

The monomer deformation energy Δ_i, the dimer interaction energy V_{ij}, and the three-body nonadditivity Δ_{ijk} was calculated using the many-body expansion described in Ref. 47.

The three-body nonadditivities were computed with the SCF/CP/aug-cc-pVDZ level. The reason why correlation energy was not considered in these calculations is that it has been shown that correlation energy is quite additive[3,48] and restriction to the uncorrelated level entails significantly less computer time. The same level of calculation was used to compute some four-body nonadditive terms in order to assess the magnitude of these contributions. They were found to be small enough—and reasonably well reproduced by the potential—to not merit the effort of adjusting to the whole four-body potential energy surface.

The sample points in the potential energy surfaces were chosen in an iterative manner. Thus, initial samples were taken from a regular scan of the hypersurface with respect to the different degrees of freedom. An initial potential parametrization was fitted to the preliminary samples and employed to predict, via numerical simulations at standard temperature, more monomers, dimers, and trimers in the gas phase as well as clusters appearing in the liquid phase. These structures were then computed at the ab initio level and added to the potential energy surface. This procedure continued until self-consistency was attained with the same accuracy as that obtained in the previous fitting. In this way, for instance, the optimal monomer energy predicted by the potential differs in only 0.06 kcal /mol with respect to that computed at the ab initio level. The final surfaces to be fitted consisted of all the polarizability and dipole moment of the optimal monomer, 555 monomer structures where both the deformation energy, relative to the optimal monomer, and the dipole were considered for fitting, 762 dimer structures where the interaction energy was fitted, and 153 trimer structures where the three-body nonadditive contributions where fitted.

The vibrational spectra presented in this work were calculated using the normal mode theory.[49] In the condensed phase, the semiclassical method suggested by Reimers and Watts for water and ice[50] was implemented. The spectra was calculated by averaging over 200 configurations taken from a Monte Carlo calculation with 500 molecules in the simulation cell. The configurations are separated by 100 000 Monte Carlo steps.

B. Model potential

The model considered in this work uses a functional form based on the MCDHO model,[4] as it allows for the inclusion of intramolecular flexibility, nonadditivity, and polarizability. The electron cloud of each atom of a molecule is represented as a negative mobile charge density with radial exponential decay, attached to a positively charged point by a harmonic oscillator to simulate the interaction between charges of atoms forming a chemical bond. All other charge-charge interactions consider all charges as points instead of densities.

The specific expression for the water-water interaction was given in Eqs. 4–6 of Ref. 4. Here we give a more general formulation, suitable to be used with larger molecules. In the following equations $r_{ij}=|\mathbf{r}_i-\mathbf{r}_j|$ is the distance between the corresponding centers, either fixed positive nuclei Z or mobile negative charges q, where i and j subscripts correspond to sites i and j.

The intramolecular energy is composed of the following terms.

(1) The electrostatic interaction between atomic centers:

$$U(Z_i,Z_j)=\frac{Z_iZ_j}{r_{ij}}. \tag{1}$$

(2) The electrostatic interaction between mobile charge densities q_i and the atomic center charge Z_j of the bonded atoms, where α_i is the intramolecular decay length of the charge density:

$$U(q_i,Z_j)=\frac{q_iZ_i}{r_{ij}}\left(1+\frac{1}{2}\exp\left(-\frac{2r_{ij}}{\alpha_i}\right)\right). \tag{2}$$

The mobile charge densities are considered as point charges when interacting with any other atomic center. In these cases the electrostatic interaction is given by

$$U(q_i,Z_j)=\frac{q_iZ_j}{r_{ij}}. \tag{3}$$

(3) The interaction between mobile charges with decay lengths α_i and α_j attached to bonded atoms. In this case a two-center integral should be used; however, an approximate expression that gives good accuracy at all relevant distances was found, i.e.,

Reuse of AIP Publishing content is subject to the terms: https://publishing.aip.org/authors/rights-and-permissions. Downloaded to IP: 150.214.182.116 On: Wed, 19 Oct 2016 14:19:58

TABLE III. Parameters of the model potential. Distances are in a.u., angles in deg, and energy is in kcal/mol. The different parameters are described in the text. R_c stands for the hard core cutoff radius used during simulation and are in a.u.

Site	Site	Site	Site	Z	q	k	
C				3.900 283	−3.408 234	569.650	1.223 331
O				0.366 121	−1.398 671	435.404	1.597 584
H_C				0.596 934	−0.601 763	602.237	0.900 642
H_O				1.990 457	−1.442 636	455.769	0.849 260
				D_{ij}		r_{ij}^{eq}	
O	C			4.595 276	0.977 601	3.997 212	
H_C	C			70.427 959	1.078 138	2.292 126	
O	H_O			21.473 454	1.584 645	2.021 717	
				k_θ		k_{UB}	r_{ik}^0
H_C	C	O		89.700	109.471	7.957	3.955
C	O	H_O		42.007	107.800	26.103	3.782
H_C	C	H_C		55.768	109.000	14.745	4.063
				k_χ	n		
H_C	C	O	H_O	0.118 728	3	0.0	
				A_{ij}	a_{ij}	B_{ij}	b_{ij}	R_c
H_C	H_O			480.231 97	0.176 31	−892.495 99	0.047 74	
C	C			97 519.618 11	2.094 63	−2.294 13	0.266 26	5.6
C	O			6 496.790 10	1.276 07	−1782.699 82	0.956 43	5.3
C	H_C			1 644.359 38	1.721 79	10.903 08	0.394 32	4.2
C	H_O			435.951 37	0.985 75	−2.765 14	0.119 54	3.7
O	O			40 041.925 58	1.065 55	−36 415.261 63	1.047 97	4.3
O	H_C			1 634.413 65	1.477 24	0.137 03	0.024 35	3.7
O	H_O			4 001.505 20	2.034 11	8.159 27	0.299 31	2.8
H_C	H_C			2 904.622 84	2.096 89	−9.006 16	0.478 64	2.83
H_C	H_O			1 114.574 06	1.201 24	−1132.260 23	1.178 35	2.83
H_O	H_O			623.490 48	1.193 27	−347.755 15	0.965 90	2.95

$$U(q_i,q_j)=\frac{q_iq_j}{r_{ij}}\left[1-\left(\frac{0.6}{0.6+\frac{a_i+a_j}{2}r_{ij}+1}\right)\exp\left(-2\frac{0.6+\frac{a_i+a_j}{2}r_{ij}+\left(\frac{a_i+a_j}{2}r_{ij}\right)^2/3}{0.6+\frac{a_i+a_j}{2}r_{ij}}\right)\right] \quad (4)$$

again the mobile charge densities are considered as point charges when interacting with mobile charge densities of nonbonded atoms

$$U(q_i,q_j)=\frac{q_iq_j}{r_{ij}}. \quad (5)$$

(4) A Morse potential between each pair of bonded atoms, with depth D_{ij}, inverse decay length α_{ij}, and equilibrium parameter r_{ij}^{eq},

$$U_b(r_i,r_j)=D_{ij}[\exp(2\alpha_{ij}(r_{ij}-r_{ij}^{eq}))-\exp(\alpha_{ij}(r_{ij}-r_{ij}^{eq}))] \quad (6)$$

(5) A quadratic plus Urey-Bradley (U_{UB}) terms for each bond angle θ_{ijk}, with parameters k_θ and k_{UB}, and the equilibrium values θ_{ijk} and r_{ik}^0,

$$U_\theta=\frac{k_\theta}{2}(\theta_{ijk}-\theta_{ijk}^0)^2 \quad (7)$$

$$U_{UB}=\frac{k_{UB}}{2}(r_{ik}-r_{ik}^0)^2 \quad (8)$$

(6) A periodic function over the dihedral angle χ between four consecutive bonded centers

$$U_{dih}=\frac{k_\chi}{2}[1+\cos(n\chi-\chi^0)] \quad (9)$$

(7) Exponential terms between the nonbonded atoms, i.e., that do not form angles or covalent bonds.

$$U_{nb}=A\exp(-ar)+B\exp(-br) \quad (10)$$

Hence the analytical expression to compute the intramolecular energy is

$$U_S=\sum_{i\in S}\sum_{j>i}U(Z_i,Z_j)+\sum_{i\in S}\sum_{j>i}U(q_i,q_j)+\sum_{i\in S}\sum_{j>i}U(q_i,Z_j)+\sum_{i\in S}\frac{1}{2}k_ir_{ii}^2+\sum_{\text{bonds}}U_b(Z_i,Z_j)+\sum_{\text{angles}}U_\theta+U_{UB}+\sum_{\text{dih}}U_{dih}+\sum_{\text{nonbond}}U_{LJ}, \quad (11)$$

where the third term corresponds to the harmonic energy of the mobile charge at a distance r_{ii} from its nucleus and the summation $i\in S$ refers to the entire molecule.

Reuse of AIP Publishing content is subject to the terms: https://publishing.aip.org/authors/rights-and-permissions. Downloaded to IP: 150.214.182.116 On: Wed, 19 Oct 2016 14:19:58

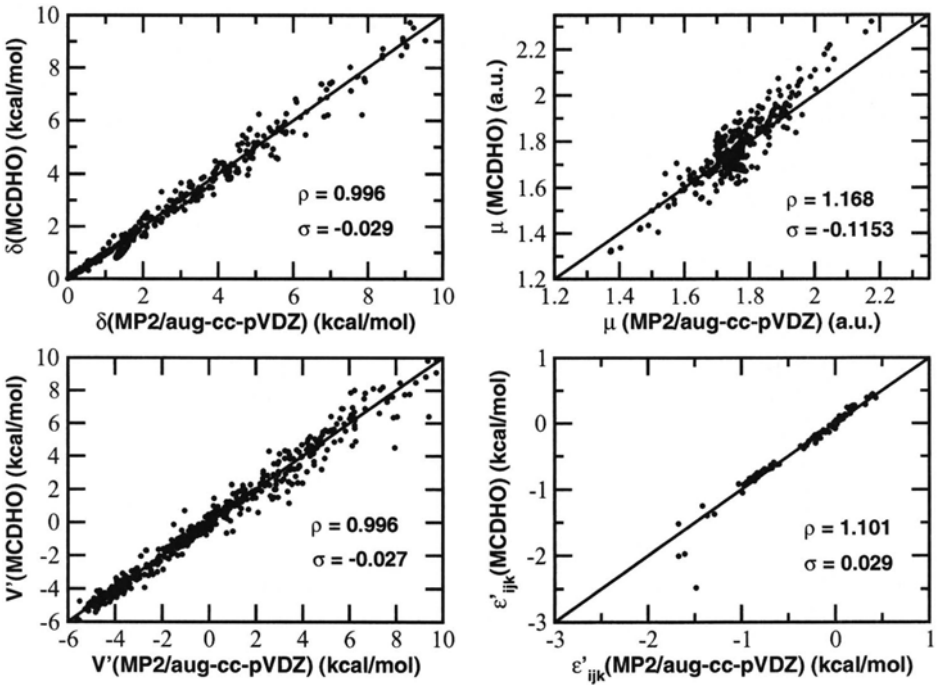

FIG. 1. Comparison between the monomer deformation energies δ_i, monomer dipole moments μ_i, dimer interaction energies as described in Ref. 47 V_{ij}, and three-body nonadditivities as described also in Ref. 47 ε'_{ijk} predicted at the ab initio level and those predicted by the model for the same structures.

The intermolecular energy is composed of the following terms.

(1) The electrostatic interactions between atomic centers plus exponential terms with parameters A_{ij}, B_{ij}, a_{ij}, and b_{ij};

$$U_{\text{inter}}(Z_i, Z_j) = A_{ij} \exp(a_{ij} r_{ij}) + B_{ij} \exp(b_{ij} r_{ij}) + \frac{Z_i Z_j}{r_{ij}}. \quad (12)$$

(2) The electrostatic interaction between mobile charges q_i considered as point charges and charges Z_j,

$$U_{\text{inter}}(q_i, Z_j) = \frac{q_i Z_j}{r_{ij}}. \quad (13)$$

(3) The electrostatic interaction between mobile charges,

$$U_{\text{inter}}(q_i, q_j) = \frac{q_i q_j}{r_{ij}}. \quad (14)$$

Therefore, the energy of a cluster with N molecules is given by

$$U = \sum_{S=1}^{N} \sum_{T=1}^{S} \sum_{i \in S} \sum_{j \in T} U_{\text{inter}}(Z_i, Z_j) + U_{\text{inter}}(q_i, Z_j) + U_{\text{inter}}(q_j, Z_i) + U_{\text{inter}}(q_i, q_j) + \sum_{S=1}^{N} U_S, \quad (15)$$

where summations $i \in S$ and $j \in T$ refer to entire molecules. The interaction energy requires the subtraction of the intramolecular energies of the isolated molecules, U_S^0,

$$U = U - \sum_{S=1}^{N} U_S^0, \quad (16)$$

thus taking into consideration the energetic cost of polarizing and deforming each molecule in the cluster or the condensed phase.

Unlike the case of water,[4] and because of the complexity of the potential energy surface due to the increased number of degrees of freedom, it was found convenient to use hard core cutoff radii for the interactions as part of the potential. So in addition to the set of parameters fitted to reproduce the surfaces, using the program VA05AD,[51] the potential definition

TABLE IV. Structural parameters for the optimal methanol monomer. Comparison of MCDHO results against ab initio and experimental results. Error bars for the MCDHO results at 298 K correspond to 2σ using the method of Flyvbjerg and Petersen, Ref. 71, for the computation of σ. Distances are in angstroms, bond and dihedral angles are in deg, and dipole moment in Debye.

Method	r_{CO}	r_{OH}	$\angle COH$	d_{HCOH}	μ
aug-cc-pVDZ	1.4342	0.9659	107.9	180.00	1.71
MCDHO (0 K)	1.4386	0.9639	107.8	180.00	1.72
MCDHO (298 K)	1.4423±0.0014	0.9667±0.0004	108.4±0.3	–	1.72±0.01
Expt.[a]	1.434	0.937	105.93	–	1.69
Expt.[b]	1.4246±0.0024	0.9451±0.0034	108.53±0.48	–	–

[a]Reference 44.
[b]Reference 72.

Reuse of AIP Publishing content is subject to the terms: https://publishing.aip.org/authors/rights-and-permissions. Downloaded to IP: 150.214.182.116 On: Wed, 19 Oct 2016 14:19:58

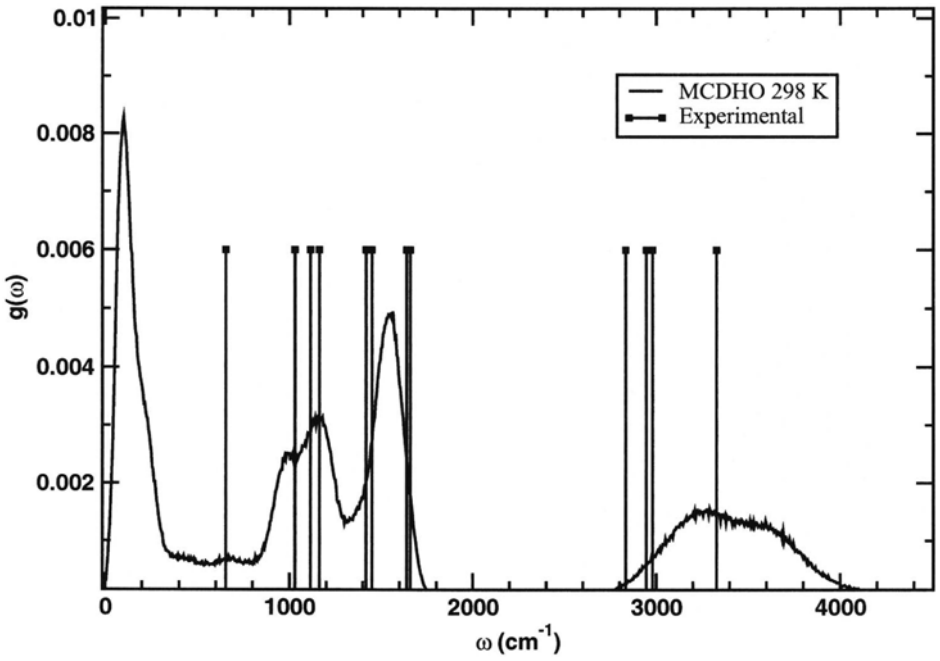

FIG. 2. Vibrational spectral density of liquid methanol, MCDHO, and experimental results.

includes a set of cutoff values. Differentiating the methyl hydrogen from the hydroxyl hydrogen also proved convenient, so they were treated as different atomic species.

III. RESULTS

A. Model potential performance

1. Reproduction of the adjusted properties

The fitted parameters for the methanol-methanol potential and the corresponding cutoff values are presented in Table III. The quality of the reproduction of the monomer deformation energy surface and dipole moment is presented in Fig. 1, as well as the two-body interactions and the three-body nonadditivity. In addition the trace of the polarizability tensor also fitted by the model comes to be α_{xx}=21.2, α_{yy}=23.3, and α_{zz}=18.8 a.u. which compares rather well to the ab initio values α_{xx}=20.5, α_{yy}=23.2, and α_{zz}=19.8 a.u. and the experimental isotropic values of α of 21.8 [Ref. 52] and 22.0 a.u.[53]

2. Reproduction of molecular clusters

A comparison between the geometries of the optimal methanol monomer predicted by the model, the corresponding ab initio monomer, and the experimental values is presented in Table IV. A very good agreement of the model with the optimal ab initio structure was found. Furthermore, the Monte Carlo simulation of the single monomer at 298 K predicts geometrical values which are very close to the experimental ones.

In Fig. 2 the vibrational spectra of the methanol molecule in the liquid phase is presented and compared to the experimental data. It was computed via a normal mode analysis. In order to estimate the reliability of this treatment we compared its predictions for the water molecule with those estimated from the velocity autocorrelation in a molecular dynamics (MD) simulation with the MCDHO potential by Stern et al.[54] We can see in Table V that the two methods yield similar results for the shift from the gas to liquid phase, giving confidence in the application of the normal mode analysis to the methanol molecule. In Table VI the vibrational spectra predicted for the methanol molecule in

TABLE V. Vibrational frequencies of water in gas and liquid phases. All frequencies are in cm^{-1}.

	Expt.		MCDHO (MD)		MCDHO (NM)		Expt.	MCDHO (MD)	MCDHO (NM)
	Gas[c]	Liquid[d]	Gas	Liquid	Gas	Liquid	Liquid-gas	Liquid-gas	Liquid-gas
OH symm. stretch	3756	3557	3918	3668	3928	3742	−150	−250	−186
OH antisymm. stretch	3657		3785	3407	3789	3346		−378	−443
HOH bend	1595	1670	1651	1740	1660	1754	75	89	94

[a]Reference 54.
[b]Normal modes. This work.
[c]Reference 73.
[d]Reference 74.

Reuse of AIP Publishing content is subject to the terms: https://publishing.aip.org/authors/rights-and-permissions. Downloaded to IP: 150.214.182.116 On: Wed, 19 Oct 2016 14:19:58

TABLE VI. Vibrational frequencies of methanol in gas and liquid phases. All frequencies are in cm^{-1}.

	aug-cc-pVDZ	Expt.[a]		MCDHO		Expt.	MCDHO
	Gas	Gas	Liquid	Gas	Liquid	Liquid-gas	Liquid-gas
O–H stretch	3839	3681	3328	3752	3679	−353	−73
d-stretch	3189	3000	2980	3540	3478	−20	−62
	3130	2960	2946	3260	3276	−14	16
CH_3 s-stretch	3052	2844	2834	3252	3101	−10	−151
CH_3 d-deform	1505	1477	1480	1592	1617	3	25
	1494	1477	1480	1538	1617	3	79
CH_3 s-deform	1466	1445	1450	1521	1557	5	36
O–H bend	1367	1345	1418	1240	1492	73	252
CH_3 d-rock	1170	1165	1163	1167	1185	−2	18
	1076	1065	1115	1116	1093	50	−23
C–O stretch	1046	1033	1030	981	973	−3	−8
Torsion	315	200–295	655	307	658	455–360	351

[a]Reference 75.

the gas and liquid phases are compared against the ab initio and experimental values. It can be seen that there is a reasonable agreement in the gas phase description, but less so for the liquid phase. In particular, the shift from gas to liquid phase for the OH bond stretch mode is much reduced.

The optimal methanol dimer predicted by the model is in very good agreement with the optimal ab initio dimer, as shown in Table VII. In Fig. 3 (inset) a superposition of ab initio and model optimum dimers is presented showing a discrepancy in a rotation along the hydrogen bond axis, something very difficult to prevent, e.g., it also occurred in the water dimer.[4] A search for an ab initio CP corrected dimer as described previously produced the parameters presented in the third column of Table VII, which show a better agreement to the experimental values. There is also an improved agreement between the model optimal dimer and the CP corrected dimer.

Of course it is important to reproduce the hydrogen bond interaction not only in the single optimal structure. In Fig. 3 the interaction energy profile for the optimal approach of the methanol monomers along the hydrogen bond is presented showing an excellent agreement between the model and the ab initio curve.

In Table VIII and Fig. 4 we compare the optimal methanol trimers predicted by the model and the ab initio calculations. In this case it was not possible to find the CP corrected optimal structure since the ab initio optimization follows the CP uncorrected surface. But the optimal trimer predicted by the model when calculated at the ab initio level with CP correction turned out to have a mere 0.14 kcal/mol difference with the one obtained by the ab initio minimization. Hence trimer structure reproduction is in good agreement with the ab initio calculation except for a small overestimation of the interaction energy and an overestimation of 0.05 Å in the oxygen-oxygen distance.

It is also important to look into the hexamer ring, since there is a discussion regarding the importance of this structure in the liquid phase of methanol, as well as a report[31] on the possibility that simple potentials do not reproduce well this structure. In Table VIII we compare some structural parameters predicted by the model and ab initio calculations at the MP2/6-31++G^{**} level for the optimal hexamer. The table shows a general agreement between both structures. There is an apparent elongation of the hydrogen bond distance in the model predicted structure, but this elongation of 0.04 Å is quite similar to the apparent elongation between the CP corrected and uncorrected structures at the ab initio level. Furthermore, the level of ab initio calculation is smaller than the one used for computing the energy surface, because of the computational cost involved, hence the agreement is quite adequate. From this it can be concluded that the model potential is reproducing the methanol clusters accurately and that it can be used to study the condensed phase.

B. Numerical simulations

The results obtained in reproducing the molecular properties, the interaction energies, and structures of small clusters support the reliability of the model potential in studies of the condensed phase. Liquid methanol simulations were carried out with the Monte Carlo Metropolis algorithm in the canonical ensemble (NVT) with periodic boundary conditions and Ewald summation. A cubic box of length 2.3437 Å with 500 molecules was used to reproduce a standard density of 0.782 g/cm^3 at 298.15 K. The procedure of updating only the polarization of the trial molecule (called single update) has been criticized for lacking the condition of detailed balance[55,56] that is sufficient but not necessary for a valid sampling;[57] however, apart from hindering the convergence of the dipole-dipole correlation function,[58] from which the dielectric constant can be computed, the single update scheme does not produce any significant error compared to algorithms that comply with detailed balance,[55,56,59,60] but substantially increase the computational cost. Thus single update has been used in this work. 100×10^6 configurations were used to attain equilibrium starting from a randomly generated configuration, and 100×10^6 configurations were used for extracting the average values. We checked that both intramolecular and intermolecular degrees of freedom were equilibrated. For this we considered separately each energy for 50×10^6 configurations and both energies were at equilibrium.

Reuse of AIP Publishing content is subject to the terms: https://publishing.aip.org/authors/rights-and-permissions. Downloaded to IP: 150.214.182.116 On: Wed, 19 Oct 2016 14:19:58

TABLE VII. Structural parameters for the minimum energy methanol dimer. Comparison of MCDHO results against ab initio results. The third column corresponds to the counterpoise corrected dimer found as described in text. Distances are in Å, bond and dihedral angles are in deg, and energy in kcal/mol.

	MCDHO	MP2/aug-cc-pVDZ	MP2/aug-cc-pVDZ Counterpoise corrected	Expt.
r(O··H)	1.940	1.887	1.967	1.96±0.02[a]
r(O··O)	2.892	2.847	2.920	—
(OH··O)	166.0	168.2	166.2	—
(HO··H)	101.5	112.7	112.4	—
d(COH··O)	159.8	132.3	131.3	—
d(OH··OC)	−53.6	−6.7	−6.4	—
U	−5.27	−5.11	−5.15	—

[a]Reference 76.

The enthalpy of vaporization was computed as

$$\Delta H_{vap} = U_{vap} - U_{liq} + RT, \quad (7)$$

where U_{vap} is the energy of the vapor phase and was calculated from a Monte Carlo simulation with a single molecule at 298 K in the same cubic box used for the liquid and using 1×10^6 configurations for equilibration and 5×10^6 configurations to average the energy of the system. The vaporization enthalpy predicted $\Delta H_{vap}=8.81\pm0.04$ kcal /mol, which compares rather well with the reported experimental value of $\Delta H_{vap}=8.946\pm0.005$ kcal /mol.[61–63]

The predicted molecular properties of the methanol molecule in the liquid phase and their experimental counterparts are presented in Table IX. There is a general agreement between the predicted and the experimental values except for the dipole moment which appears to be underestimated. However, there is an ample discussion in the literature suggesting that the experimental value of 2.85 D is overestimated. Pieruccini and Saija[64] considered that the dielectric constant of 33 indicates a dipole in the liquid of 2.39 D. The same value has been proposed by Wick and Dang[65] in a classical simulation and Handgraff and Meijer[66] in a Car and Parinello simulation. Similarly Weerasinghe and Smith.[67] with an empirical model and Martín et al.[38] in a quantum mechanics/molecular mechanic simulation propose a value of 2.4 D. In summary the value predicted by the model is quite good and therefore all properties of the molecule in the liquid are well reproduced.

The total radial distribution function predicted by the model was estimated and compared with those of Yamaguchi et al.[25] and Adya et al.[26] in Fig. 5. The first two curves were constructed from the partial radial distribution functions using the weighting scheme suggested by Adya et al.[26] In Fig. 5 the comparison shows that the disagreement between the

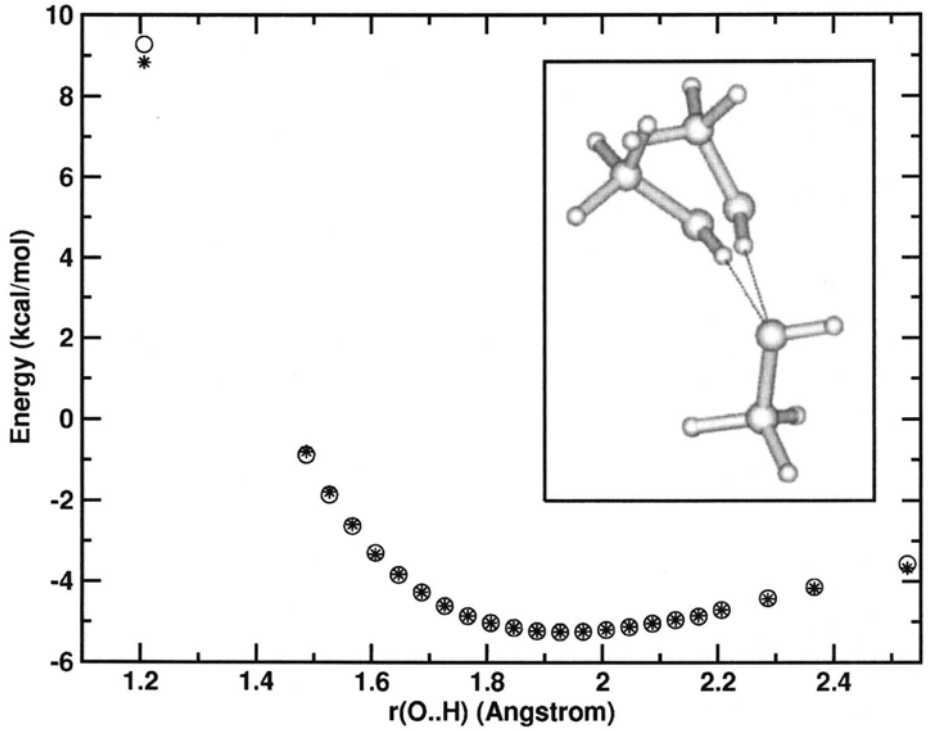

FIG. 3. Methanol-methanol dimer interaction energy along the hydrogen bond approaching line. MCDHO predicted values (stars) vs ab initio results (circles). Inset: optimal methanol dimer predicted by the model (top right) and the ab initio (top left) one. The geometries were superimposed on the oxygen atom and as close as possible to the oxydryl hydrogen and the carbon atom of the bottom monomer.

Reuse of AIP Publishing content is subject to the terms: https://publishing.aip.org/authors/rights-and-permissions. Downloaded to IP: 150.214.182.116 On: Wed, 19 Oct 2016 14:19:58

TABLE VIII. Structural parameters for the optimal methanol trimer. Comparison between MCDHO and ab initio results at the MP2/aug-cc-pVDZ counterpoise corrected level (left columns) and geometrical parameters for the methanol hexamers (right columns). Ab initio MP2/6-31++G** and MCDHO results. O_a and O_d stand for the acceptor and donor oxygen in the hydrogen bonds. Distances are in Å, bond and dihedral angles are in deg, and energies in kcal/mol. The model values correspond to the average and standard deviation values produced by slightly different geometries observed in the hexamer.

	Trimer			Ring hexamer		Chain hexamer	
	MCDHO	Ab initio		MCDHO	Ab initio	MCDHO	Ab initio
r(O··H)	1.909	1.853	r(O–O)	2.72±0.01	2.68		
r(O··H)	1.959	1.881	(O–O–O)	109.5±4.1	117.5		
r(O··H)	1.889	1.860	(O_a–O_d–C)	108.2±1.7	106.3		
r(O··O)	2.819	2.766	(O_d–O_a–C)	113.5±3.6	119.4		
r(O··O)	2.853	2.790	d(O–O–O–O)	59.7±6.5	30.7		
r(O··O)	2.800	2.766	d(C–O–O–C)	167.7±6.2	123.1		
(C–O··H)	120.90	127.303					
(C–O··H)	113.14	109.864					
(C–O··H)	113.29	109.864					
d(O–H··O–H)	−6.51	−14.022					
d(O–H··O–H)	−4.48	−7.972					
d(O–H··O–H)	2.81	−7.888					
(U)	−16.18	−15.22		−42.89	−43.77	−28.15	−29.58

theoretical and the experimental lines is similar to that shown between both experimental curves. This supports the validity of the potential; even if the theoretical peak is still slightly shifted towards longer distances.

We can go further and look into the radial distribution functions for different atomic pairs and compare to the experimentally derived curves of Yamaguchi et al.[25] (Figs. 6 and 7). There is a general agreement of the model radial distribution functions to those obtained from the experiment, except for the oxygen-oxygen radial distribution function, the one involved in the hydrogen bonding between methanol molecules, where the model presents a first peak at a distance about 0.1 Å longer compared with the curves presented by Yamaguchi et al.,[25] and 0.08 Å longer compared to the curve derived from the data presented by Adya et al.[26] There is also a marked difference in the first minimum and the second peak, the experimental curve being more structured. These discrepancies are rather surprising considering the good agreement with all previous comparisons, either with ab initio or experimental counterparts. The possibility that the potential was not properly reproducing the nonadditivity in long hydrogen bonded structures, as suggested by Kashtanov et al.,[31] was considered, but it was shown that hexamers were properly reproduced. We also considered the fact that nonadditivity at the MP2 level was not computed because it is known that correlation energy is highly additive,[48] but the possibility remains that, in these cases, these corrections were not negligible. Xantheas[68] reported a substantial effect of MP2 corrections on water nonadditivity, but in that work a comparison is made between the optimal structures of the trimer predicted at the MP2 and those predicted at the self-consistent field (SCF) level; indeed, pair interaction and thus MP2 is crucial for structure determination, leading to different structures with different nanoadditivity values. Nonetheless in order to check if this could be a source of error, we computed the three-body nonadditivity surface at the MP2 level and compared it with the corresponding SCF surface. No meaningful difference appeared at any point. We also considered the possibility that the cell size was not large enough and it was hindering the formation of larger clusters. However, the radial distribution functions obtained with a cell containing 1000 molecules rendered the same results as those from the cell containing 500 molecules. It is clear that discrepancies between theoretical and experimental radial distribution functions are related to the hydrogen bonding. In a recent work it has been shown that both the radial distribution functions and the dipole moment are quite sensitive to pressure.[65] Hence the observed differences could be due to a diminished pressure in the NVT simulation at the fixed experimental density. In order to check this a NPT simulation of the same system was performed at 1 atm. The results show that the density obtained increases 0.03 g/cm^3 with respect to the previous experimental value of 0.782 g/cm^3, and the vaporization enthalpy becomes ΔH_{vap} = 8.99 kcal/mol, getting closer to the experimental value. But the radial distribution functions did not change in any appreciable manner.

The only remaining explanation would be that since the level of ab initio calculations is slightly underestimating the binding energy, this would conduce to less compact structures. We have to recall that a small shift for the OH bond stretch mode was predicted between the gas and liquid phases, a deficiency that could be involved in the discrepancy observed. However, it is surprising that the vaporization energy is well reproduced being a very sensitive parameter. It could also be that the experimental biatomic radial distribution functions are reflecting some model dependency since the empirical potential structure refinement approach was used.[25]

The model oxygen-oxygen radial distribution function indicates well defined first neighbors, but less defined second neighbors when compared to the equivalent water radial dis-

Reuse of AIP Publishing content is subject to the terms: https://publishing.aip.org/authors/rights-and-permissions. Downloaded to IP: 150.214.182.116 On: Wed, 19 Oct 2016 14:19:58

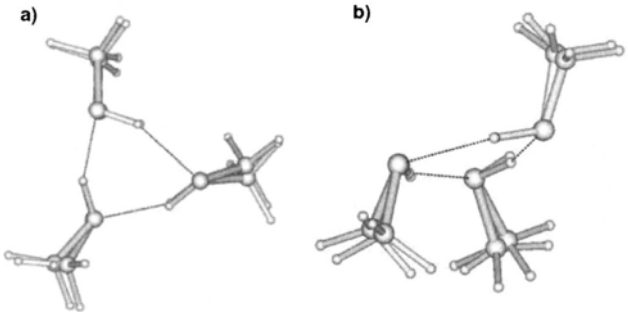

FIG. 4. Superposition of the trimer structures predicted ab initio and by the MCDHO model. Top (a) and lateral (b) views. Trimer superposition was done requesting superposition of the oxygen atoms by the molden program (Ref. 78).

tribution function, see, for example, Ref. 4. This suggests direct hydrogen bonding between the methanol molecules but not a tridimensional network as in the case of water. This agrees with the oxygen-hydroxyl hydrogen radial distribution function; the second peak is much smaller than its water counterpart. As a matter of fact, the solvation number of the first shell for the oxygen-oxygen radial distribution function is 2.1 which compares rather well with the experimental value of 1.77 ± 0.07,[25] a value smaller than the 4.5 corresponding to water. Hence contrary to water, liquid methanol does not seem to make a three-dimensional (3D) network, but rather linear polymers.

With the results of the simulation it is possible to look into the existence of chains or rings of hydrogen bonded methanol molecules. Here, methanol linked molecules have been defined as such when alternated donor-acceptor hydrogen bonds were formed between them. Bifurcated hydrogen bonds were not considered for defining linkage, so that chains that could be joined by a bifurcated hydrogen bond were considered as independent polymers. In Fig. 8 one hexameric ring and one linear polymer found in the simulation box are shown. In Fig. 9 a histogram of the relative frequency of appearance of the different polymers, either chains or rings is presented. This histogram was constructed by averaging 100 snapshots taken each 100 000 configurations and refers to the average number of clusters that occur in the simulation cell scaled by the number of molecules. A considerable amount of linear polymerization can be appreciated since fairly long chains appear. Even if the relative appearance of rings versus chains is small (4%) the number of rings is important, taking into account that only 500 molecules were used in the simulation. Formation of rings could be frustrated by the size of the simulation cell. In order to check this, a simulation using 1000 molecules that increase the cell size slightly was performed. In this case the histogram corresponding to the linear chains is unaffected, whereas the one corresponding to rings has a different profile. The most common ring changes from 4 to 5 molecules. It could be that a larger cell size will predict a more frequent occurrence of rings with n=6 or larger, in agreement with Wilson et al.[69] However, long chains, like the one presented in Fig. 8, give rise to faux rings, i.e., compact closed structure which are not really closed by hydrogen bonds and therefore they could be misleading the experimental interpretation.

It could be thought that the good performance of the potential is due to the inclusion of polarizability and intramolecular relaxation. As a matter of fact, there are several simulations including polarizability that have reproduced well the experimental data.[35–38,66] Furthermore, in two of these works[35,38] there was a comparison between the results produced by the potentials with and without polarization, indicating the need of polarization, even if some overstructuring could be occurring.[36,38] In the present model it is possible to turn off some molecular properties while keeping the same force field parameters, henceforth making the elucidation of the need of such property independent of a change in potential. Keeping the mobile charges fixed at certain positions would freeze a particular charge distribution, hence, for instance, its dipole, and then a nonpolarizable potential can be used. Similarly, fixing the intramolecular internuclear distances will lead to a rigid potential. Since in both cases the particular structures are just restricting the adjusted hypersur-

TABLE IX. Average properties of the liquid methanol predicted by different forms of the model potential as described in the text and compared to experiment. Distances are in Å, bond angles are in deg, dipole moment in D, and energies in kcal/mol. Error bars for the MCDHO results at 298 K were calculated as 2σ using the method of Flyvbjerg and Petersen, Ref. 71.

Method	r_{CO}	r_{OH}	$\angle COH$	μ	U_H
Expt.	1.415 ± 0.003[a]	0.961 ± 0.001[a]	111.0 ± 3[a]	2.85[b]	-8.946 ± 0.005[c]
	1.4246[a]	0.9451[a]	108.54[a]		
	1.43 ± 0.05[d]	0.99 ± 0.01[d]	112 ± 3[d]		
	1.42 ± 0.04[e]	1.027 ± 0.008[e]	103.4 ± 1.2[e]		
Fully flexible	1.4457 ± 0.001	0.9751 ± 0.0001	107.22 ± 0.04	2.385 ± 0.002	-8.81 ± 0.04
Rigid pol. (gas. prop.)				2.281 ± 0.008	-8.78 ± 0.04
Rigid nonpol. (gas. prop.)				1.71	-6.73 ± 0.07
Rigid pol. (liq. prop.)				2.309 ± 0.002	-8.68 ± 0.006
Rigid nonpol. (liq. prop.)				2.309	-8.44 ± 0.05

[a]Reference 26.
[b]Reference 77.
[c]References 61–63.
[d]Reference 28.
[e]Reference 27.

Reuse of AIP Publishing content is subject to the terms: https://publishing.aip.org/authors/rights-and-permissions. Downloaded to IP: 150.214.182.116 On: Wed, 19 Oct 2016 14:19:58

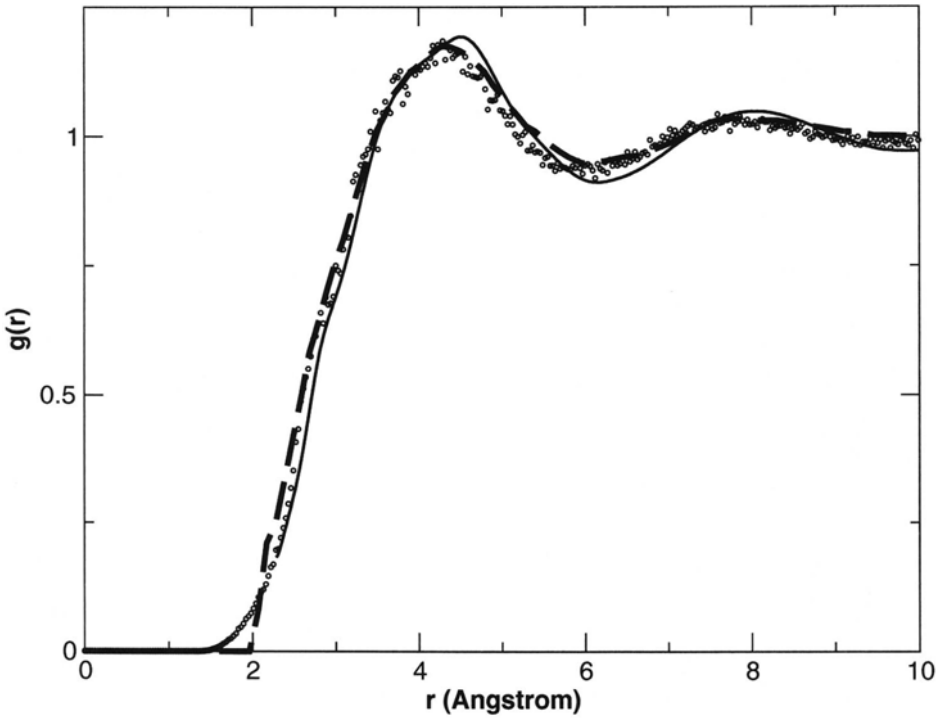

FIG. 5. Methanol weighted sum of radial distribution functions for X–X atoms. Experimental data from Adya et al. (Ref. 26) (dashed line), experimental data from Yamaguchi et al. (Ref. 25) (circles), and the MCDHO predicted curve (continuous line). Weights were taken from Adya et al. (Ref. 26).

face, there is no need for any change in the force field parameters. This idea was used to analyze the effect of the molecular properties in the performance of a water potential[58] and also to propose the construction of effective potentials through the use of effective molecular properties rather than the use of an effective force field. Here the same idea is tested for the methanol potential.

In Table IX the vaporization enthalpies and the dipole moments predicted by the fully flexible potential, and several other model potentials are presented: a rigid polarizable potential and a rigid nonpolarizable potential using the gas phase properties as well as a rigid polarizable potential and a rigid nonpolarizable potential using the liquid methanol properties. The rigid polarizable models with either the gas or the liquid methanol geometry produces a vaporization enthalpy slightly smaller but still close to the experimental value. The dipolar moment predicted by these models is smaller than that of the fully flexible due to the rigid con-

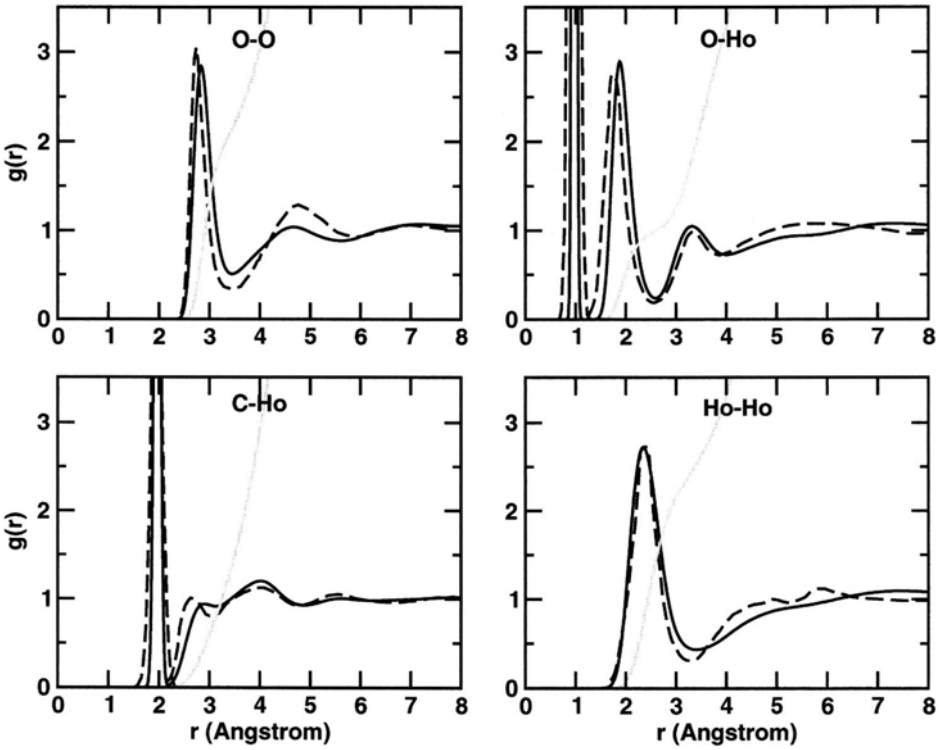

FIG. 6. Radial distribution functions for liquid methanol and solvation number (gray line). MCDHO predicted curves (continuous lines) compared to the experimental curves (dashed lines) of Yamaguchi et al. (Ref. 25).

Reuse of AIP Publishing content is subject to the terms: https://publishing.aip.org/authors/rights-and-permissions. Downloaded to IP: 150.214.182.116 On: Wed, 19 Oct 2016 14:19:58

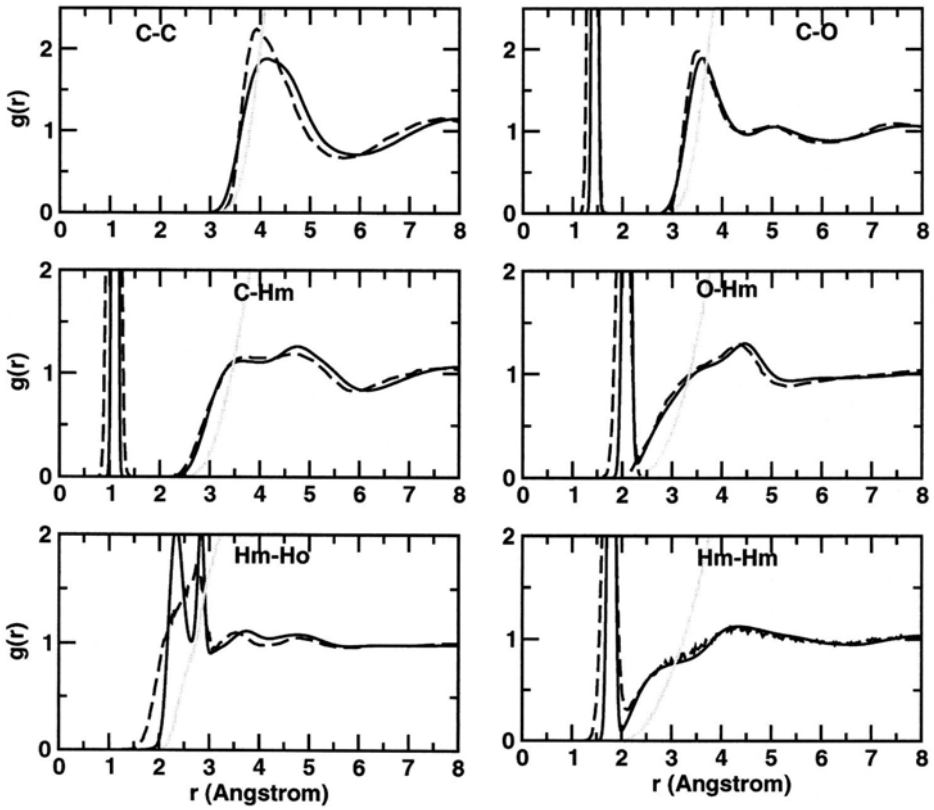

FIG. 7. Radial distribution functions for liquid methanol and solvation number (gray line: MCDHO predicted curves (continuous lines) compared to the experimental curves (dashed lines) of Yamaguchi et al. (Ref. 25).

figuration of the molecule. Obviously, the similar performance is due to the very small change in geometry from gas to liquid phase. The rigid nonpolarizable model with gas phase dipole moment produces a vaporization enthalpy much reduced. If the liquid average dipole is used instead of the gas phase one, the rigid polarizable model still yields a value close to the fully flexible potential. It is interesting that intramolecular flexibility of methanol is not critical.

In Fig. 10 the oxygen-oxygen radial distribution functions predicted by the above models are presented. The rigid polarizable models yield distribution functions almost indistinguishable between them and very similar to the fully flexible, whereas the rigid nonpolarizable model with the gas

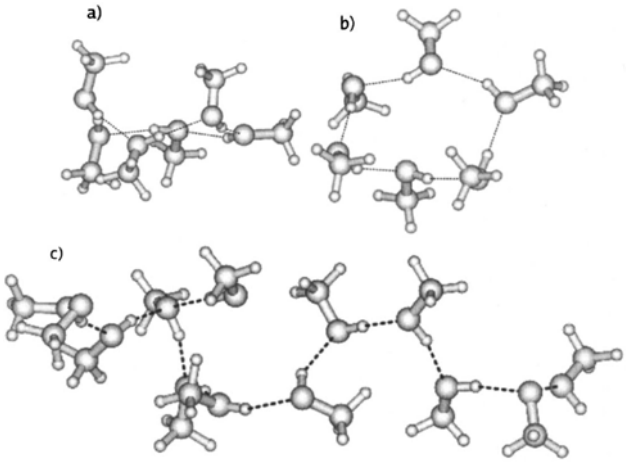

FIG. 8. Examples of hexameric rings (a) and (b) and linear polymers (c) extracted from the liquid methanol simulation box.

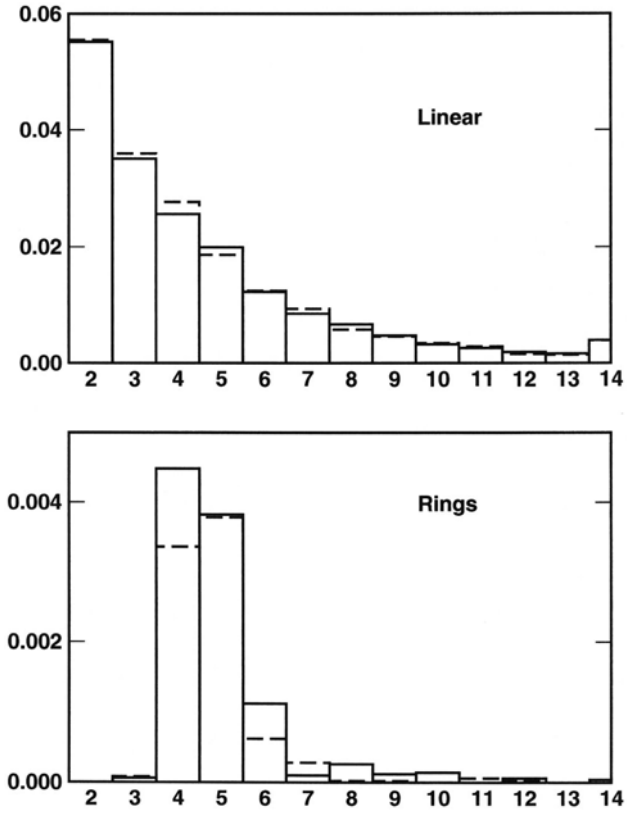

FIG. 9. Average number of linear chains and cyclic rings clusters appearing in 100 snapshots that occurred each 100 000 configurations, scaled by the number of molecules. Continuous line from simulation with 500 molecules. Broken line from simulation with 1000 molecules.

Reuse of AIP Publishing content is subject to the terms: https://publishing.aip.org/authors/rights-and-permissions. Downloaded to IP: 150.214.182.116 On: Wed, 19 Oct 2016 14:19:58

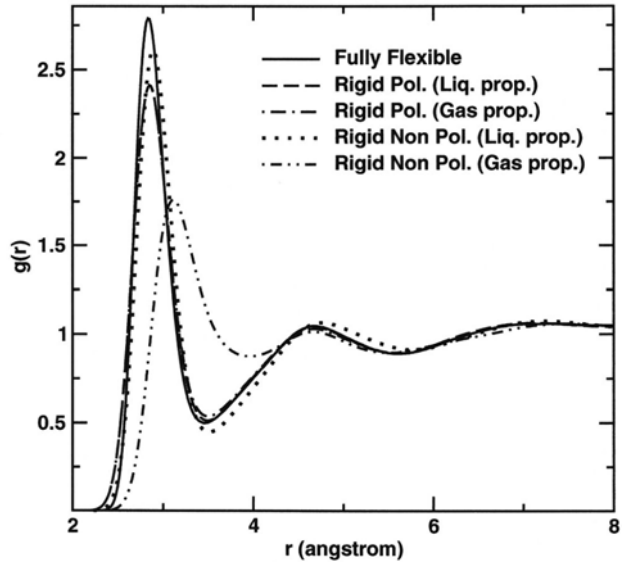

FIG. 10. Radial distribution functions predicted with the MCDHO models with different degrees of freedom.

phase dipole yields a function poorly structured. When the liquid properties are used for the rigid nonpolarizable model the structure function is greatly improved and it is now very similar to that obtained with the fully flexible model. Hence for the proper reproduction of liquid methanol a polarizable model is required either by including polarizability in the potential or modifying the molecular property to include the liquid value of the dipole in the case of methanol and dipole and geometry in the case of water.[58] Effective pair potentials can be constructed to yield reasonable, or even good reproductions of the liquid phase[67] but they certainly will not reproduce the interaction of small clusters or respond to thermodynamic conditions different from those used to construct the effective potentials.[13]

IV. CONCLUSIONS

A methanol-methanol potential derived from ab initio calculations has been presented. This potential has been proven to reproduce the molecular properties as well as the structure and interaction energies of small clusters. The liquid methanol properties are well reproduced, except for small discrepancies in the radial distribution functions.

It is also clear that there is an absolute need for a polarizable model, or an effective model that has taken polarizability into account, for the proper description of the system.

There is a good agreement between the structural and energetic values of the model clusters and the ab initio prediction, but the model has a tendency to yield slightly less compact structures and slightly less favorable energy, in clusters and in the liquid phase.

An analysis of the different types of clusters that appear in the liquid phase shows that both chains and rings appear, chains are able to grow to considerable size, and rings can grow up to heptamers, even if less frequently. This agrees with the NMR Ref. 70 and x-ray absorption[69] observations and explains how the highly structured network of methanol molecules is responsible for the peculiar properties of the substance without resulting in a waterlike 3D network.

ACKNOWLEDGMENTS

This work was supported by CONACyT Grant No. V50479-R and DGAPA-UNAM Grant No. IN111706. We are grateful to Reyes Garcia Carreon for his help in the computational part of this work.

[1] H. Saint-Martin, C. Medina-Llanos, and I. Ortega-Blake, J. Chem. Phys. 93, 6448 (1990)
[2] J. M. Martínez, J. Hernández-Cobos, H. Saint-Martin, R. R. Pappalardo, I. Ortega-Blake, and E. Sánchez-Marcos, J. Chem. Phys. 112, 2339 (2000)
[3] M. Carrillo-Tripp, H. Saint-Martin, and I. Ortega-Blake, J. Chem. Phys. 118, 7062 (2003)
[4] H. Saint-Martin, J. Hernández-Cobos, M. I. Bernal-Uruchurtu, I. Ortega-Blake, and H. J. C. Berendsen, J. Chem. Phys. 113, 10899 (2000)
[5] P. Y. Ren and J. W. Ponder, J. Phys. Chem. B 107, 5933 (2003)
[6] R. Ayala, J. Martínez, R. Pappalardo, H. Saint-Martin, I. Ortega-Blake, and E. Sánchez-Marcos, J. Chem. Phys. 117, 10512 (2002)
[7] R. Ayala, J. Martinez, R. Pappalardo, and E. Sanchez-Marcos, J. Chem. Phys. 119, 9538 (2003)
[8] M. W. Mahoney and W. L. Jorgensen, J. Chem. Phys. 112, 8910 (2000)
[9] C. J. Burnham, J. C. Li, S. S. Xantheas, and M. Leslie, J. Chem. Phys. 110, 4566 (1999)
[10] S. W. Rick, S. J. Stuart, and B. J. Berne, J. Chem. Phys. 101, 6141 (1994)
[11] J. Hernández-Cobos, I. Ortega-Blake, M. Bonilla-Marín, and M. Moreno-Bello, J. Chem. Phys. 99, 9122 (1993)
[12] J. Hernández-Cobos and I. Ortega-Blake, J. Chem. Phys. 103, 9261 (1995)
[13] J. Hernandez-Cobos, H. Saint-Martin, A. Mackie, L. Vega, and I. Ortega-Blake, J. Chem. Phys. 123, 044506 (2005)
[14] G. Olah, A. Goeppert, and G. Prakash, Beyond Oil and Gas: The Methanol Economy (Wiley-VCH, Weinheim, 2006)
[15] B. M. Ladanyi and M. S. Skaf, Annu. Rev. Phys. Chem. 44, 335 (1993)
[16] B. H. Torrie and S. X. Weng, Mol. Phys. 67, 575 (1989)
[17] K. J. Tauer and W. N. Lipscomb, Acta Crystallogr. 5, 606 (1952)
[18] M. Haughney, M. Ferrario, and I. R. McDonald, J. Phys. Chem. 91, 4934 (1987)
[19] W. L. Jorgensen, J. Am. Chem. Soc. 103, 134 (1981)
[20] E. Tsuchida, Y. Kanada, and M. Tsukada, Chem. Phys. Lett. 311, 236 (1999)
[21] J. W. Haandgraaf, T. S. van Erp, and E. J. Meijer, Chem. Phys. Lett. 367, 617 (2003)
[22] J. A. Morrone and M. E. Tuckerman, J. Chem. Phys. 117, 4403 (2002)
[23] M. Pagliali, G. Cardini, R. Righini, and V. Chettino, J. Chem. Phys. 119, 6655 (2003)
[24] T. Yamaguchi, K. Hidaka, and A. K. Soper, Mol. Phys. 96, 1159 (1999)
[25] T. Yamaguchi, K. Hidaka, and A. K. Soper, Mol. Phys. 97, 603 (1999)
[26] A. K. Adya, L. Bianchi, and C. J. Wormald, J. Chem. Phys. 112, 4231 (2000)
[27] D. G. Montague, I. P. Gibson, and J. C. Dore, Mol. Phys. 44, 1355 (1981)
[28] Y. Tanaka, N. Ohtomo, and K. Arakawa, Bull. Chem. Soc. Jpn. 58, 644 (1984)
[29] A. H. Narten and A. Habenschuss, J. Chem. Phys. 80, 3387 (1984)
[30] M. Magini, G. Paschina, and G. Piccaluga, J. Chem. Phys. 77, 2051 (1982)
[31] S. Kashtanov, A. Augustson, J. Rubensson, J. Nordgren, H. Ågren, J. H. Guo, and Y. Luo, Phys. Rev. B 71, 104205 (2005)
[32] T. Kosztolnyi, I. Bak, and G. Palinks, J. Chem. Phys. 118, 4546 (2003)
[33] J. Gao, D. Habibollazadeh, and L. Shao, J. Phys. Chem. 99, 16460 (1995)
[34] L. Bianchi, A. K. Adya, O. N. Kalugin, and C. J. Wormald, J. Phys.: Condens. Matter 11, 9151 (1999)
[35] A. Sum, S. Sandler, R. Bukowski, and K. Szalewicz, J. Chem. Phys. 116, 7627 (2002)
[36] H. Yu, D. Geerke, H. Liu, and W. van Gunsteren, J. Comput. Phys. 27, 1494 (2006)
[37] S. Patel and C. L. BrooksIII, J. Chem. Phys. 122, 024508 (2005)

Reuse of AIP Publishing content is subject to the terms: https://publishing.aip.org/authors/rights-and-permissions. Downloaded to IP: 150.214.182.116 On: Wed, 19 Oct 2016 14:19:58

[38] M. Martín, M. Sánchez, F. O. del Valle, and M. Aguilar, J. Chem. Phys. 116, 1613 (2002).
[39] M. J. Frisch, G. W. Trucks, H. B. Schlegel et al. GAUSSIAN 98, Revision A.7, Gaussian, Inc., Pittsburgh, PA, 1998.
[40] D. E. Woon and T. H. Dunning, J. Chem. Phys. 98, 1358 (1993). See URL: http://link.aip.org/link/?JCP/98/1358/1
[41] R. A. Kendall, T. H. Dunning, and R. J. Harrison, J. Chem. Phys. 96, 6796 (1992). See URL: http://link.aip.org/link/?JCP/96/6796/1
[42] T. H. Dunning, J. Chem. Phys. 90, 1007 (1989). See URL: http://link.aip.org/link/?JCP/90/1007/1
[43] J. Wang, R. Boyd, and A. Laaksonen, J. Chem. Phys. 104, 7261 (1996).
[44] E. V. Ivash and D. M. Dennison, J. Chem. Phys. 21, 1804 (1953).
[45] S. Tsuzuki, T. Uchimaru, K. Matsumura, M. Mikami, and K. Tanabe, J. Chem. Phys. 110, 11906 (1999). See URL: http://link.aip.org./link/?JCP/110/11906/1
[46] M. Kone, B. Illien, J. Graton, and C. Laurence, J. Phys. Chem. A 109, 11907 (2005).
[47] N. Pastor and I. Ortega-Blake, J. Chem. Phys. 99, 7899 (1993).
[48] V. F. Lotrich and K. Salewicz, J. Chem. Phys. 106, 9668 (1997).
[49] E. B. Wilson , J. C. Decius, and P. C. Cross, Molecular Vibrations Dover, New York, 1980.
[50] J. Reimers and R. Watts, Chem. Phys. 91, 201 (1984).
[51] M. J. F. Powell, Harwell Subroutine Library, 1969.
[52] A. Maryott and F. Buckley, Natl. Bur. Stand. Circ. (U. S.) 537 (1953).
[53] E. Ivanov and V. Abrosimov, Russ. Chem. Bull. 54, 1987 (2005).
[54] H. A. Stern, F. Rittner, B. J. Berne, and R. A. Friesner, J. Chem. Phys. 115, 2237 (2001).
[55] M. G. Martin, B. Chen, and J. I. Siepmann, J. Chem. Phys. 108, 3383 (1998).
[56] M. Předota, P. T. Cummings, and A. A. Chialvo, Mol. Phys. 99, 349 (2001).
[57] V. I. Manousiothakis and M. W. Deem, J. Chem. Phys. 110, 2753 (1999).
[58] H. Saint-Martin, J. Hernández-Cobos, and I. Ortega-Blake, J. Chem. Phys. 122, 224509 (2005).
[59] B. Chen, J. J. Potoff, and J. I. Siepmann, J. Phys. Chem. B 104, 2378 (2000).
[60] M. Předota, P. T. Cummings, and A. A. Chialvo, Mol. Phys. 100, 2703 (2002).
[61] J. Polak and G. Benson, J. Chem. Thermodyn. 3, 235 (1971).
[62] R. C. Wilhoit and B. J. Zwolinski, J. Phys. Chem. Ref. Data 2, 2 (1973).
[63] B. P. Sahli, H. G. Gager, and A. J. Richard, J. Chem. Thermodyn. 8, 179 (1976).
[64] M. Pieruccini and F. Saija, J. Chem. Phys. 121, 3191 (2004).
[65] C. D. Wick and L. X. Dang, J. Chem. Phys. 123, 184503 (2005).
[66] J.-W. Handgraaf and E. J. Meijer, J. Chem. Phys. 121, 10111 (2004).
[67] S. Weerasinghe and P. E. Smith, J. Phys. Chem. 109, 15080 (2005).
[68] S. Xantheas, J. Chem. Phys. 100, 7523 (1994).
[69] K. Wilson, M. Cavalleri, B. Rude, R. Schaller, T. Catalano, A. Nilsson, R. Saykally, and L. Petterson, J. Phys. Chem. B 109, 10194 (2005).
[70] J. Guo, Y. Luo, A. Augustsson, S. Kashtanov, J.-E. Rubensson, D. K. Shuh, H. Agren, and J. Nordgren, Phys. Rev. Lett. 91, 157401 (2003). See URL: http://link.aps.org/abstract/PRL/v91/e157401
[71] H. Flyvbjerg and H. G. Petersen, J. Chem. Phys. 91, 461 (1989).
[72] R. M. Lees and J. G. Baker, J. Chem. Phys. 48, 5299 (1968).
[73] G. Hertzberg, Electronic Spectra and Electronic Structure of Polyatomic Molecules Van Nostrand Reinhold, New York, 1996.
[74] S.-H. Chen, K. Toukan, C.-K. Loong, D. L. Price, and J. Teixeira, Phys. Rev. Lett. 53, 1360 (1984).
[75] T. Shimanouchi, Tables of Molecular Vibrational Frequencies (U.S. Department of Commerce, Washington, D.C., 1972), Vol. 1.
[76] F. J. Lovas and H. Hartwig, J. Mol. Spectrosc. 185, 98 (1997).
[77] A. McClellan, Tables of Experimental Dipole Moments (Rahara Enterprises, El Cerrito, 1989).
[78] G. Schaftenaar and J. Noordik, J. Comput.-Aided Mater. Des. 14, 123 (2000).

Reuse of AIP Publishing content is subject to the terms: https://publishing.aip.org/authors/rights-and-permissions. Downloaded to IP: 150.214.182.116 On: Wed, 19 Oct 2016 14:19:58